

# Brazed Diamond Micropowder Bur Fabricated by Supersonic Frequency Induction Heating for Precision Machining

Bojiang Ma, Jianpeng Lou, and Qian Pang

(Submitted November 22, 2013; in revised form January 12, 2014; published online February 25, 2014)

The common brazed diamond micropowder bur fabricated in a vacuum furnace produces an even brazing alloy surface. The small brazed diamond grits show low outcropping from the brazing alloy surface, and the chip space between them is small. The bur shows a low grinding efficiency and poor heat dissipation. In this study, a brazed diamond micropowder bur was fabricated by supersonic frequency induction heating. The method afforded a fluctuant surface on the brazing alloy. The brazed diamond grits with an outcropping height distributed uniformly on the fluctuant surface. The fluctuant surface showed a certain chip space. These characteristics of the tool increased the grinding efficiency and decreased the temperature of the grinding arc area. The roughness  $R_a$  of the ceramic tile surface trimmed by the tool cylinder was between 0.09 and 0.12  $\mu\text{m}$ . In the first 90 min, the decrease in the weight of the ceramic tile ground by the tool cylinder was higher than that ground by the tool fabricated in a vacuum furnace. When the ceramic tile was cylindrically ground, the temperature of the grinding arc area measured using a thermocouple remained below 70 °C.

**Keywords** bur, diamond micropowder, induction brazing, Ni-based brazing alloy, surface

## 1. Introduction

The grinding efficiency of a brazed diamond micropowder bur is slightly lower than that of a brazed big-diamond-grit bur; however, it is used predominantly in precision processing such as trimming tooth, polishing dental materials, restoring cultural relic, and internal grinding of jade. The strike of light diamond grits is not harmful to the mouth if the grits fall off from brazed diamond micropowder bur during trimming tooth. The trimmed artifacts have a high degree of finish owing to fine diamond grits. The brazed diamond micropowder bur has low vibration during operation; therefore, accidental damage to trimmed artifacts is greatly lowered or pain is alleviated during the dental work.

The brazing of diamond is aimed to form firm metallurgical bonding between diamond grits and brazing alloy; therefore, the brazing alloy used must contain active elements that can chemically react with carbon. The wetting of brazing alloy with active elements greatly increases its bonding to diamond grits. However, the brazing alloy may completely cover the small diamond grits under long-time heating and elevated temperature conditions, thus decreasing the machinability of the diamond grits (Ref 1, 2). The brazing temperature can be

controlled and the brazing time can be shortened by supersonic frequency induction heating; therefore, it was chosen as the heating mode in this study.

A large chip space can be obtained by a high protrusion of brazed diamond grits for the brazed big-diamond-grit bur used for high efficiency and heavy load machining (Ref 3, 4). However, small diamond grits appear on the brazing alloy surface of the brazed diamond micropowder bur fabricated in a vacuum furnace. The small diamond grits have a low protrusion and limited chip space between them, which prevents heat dissipation and cause surface burning of the machined workpiece. A porous metal bond is usually adopted to solve this problem (Ref 5, 6); however, porous microstructures can lower the strength of metal bond and its hold to diamond grits.

An alternating magnetic field produces a fluctuating metal-free liquid surface during the high-frequency induction melting of metal (Ref 7, 8). Therefore, a fluctuant surface can be formed on the brazing alloy surface using alternating magnetic field. The valley of a fluctuant surface can store grinding fluid and chip; therefore, it may help in the heat dissipation of the brazed diamond micropowder bur when in use. The grinding force is also greatly lowered because of the decrease in the contact area between the brazed diamond micropowder bur and workpiece.

## 2. Experimental

### 2.1 Sample Preparation

A man-made diamond micropowder of diameter 30–40  $\mu\text{m}$  was used as the abrasive material. Ni-based alloy powder (200–300 mesh; Cr: 10 wt.%, B: 2.1 wt.%, Si: 4 wt.%, Ni: balance) was used as the brazing alloy. The substrate used was a 1045 steel cylinder (diameter: 8 mm) with a hemispherical cap of

Bojiang Ma, Jianpeng Lou, and Qian Pang, College of Electromechanical Engineering, Qingdao University of Science & Technology, Qingdao 266061, P. R. China. Contact e-mail: mbj2004@sina.com.

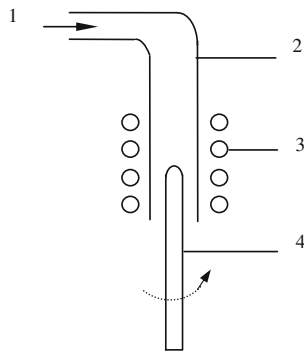


**Fig. 1** Schematic of the induction brazing device: (1) gas input; (2) quartz tube; (3) inductor; (4) rotating bur

radius 4 mm at one end. A solution was prepared from acetone and acrylic adhesive in a ratio of 20:1. The 15 mm long part from a hemispherical cap top was vertically immersed in the solution and dried. The part was uniformly coated with a layer of brazing alloy (135 mg). Then, the solution was sprayed on the part and dried. Finally, the part was uniformly coated with a layer of diamond micropowder (22 mg).

## 2.2 Device and Processing

The brazing of the diamond micropowder was carried out in the heating device shown as Fig. 1. The inductor (inner diameter: 300 mm) was made of four turns of a hollow copper tube (outer diameter: 8 mm; inner diameter: 4 mm). The heating power was determined by the coupling gap between the outer circle of the workpiece and the inner circle of the inductor. It is difficult to achieve an even coupling gap. In the experiment, the workpiece rotated at a rotating speed of 1.5 rps to get an even temperature. The power of the supersonic induction power source used was 15 kW, its oscillation frequency was 15–35 kHz, and its output induction current was 550 Å. An infrared thermometer with a range of 1500 °C was used to measure the brazing temperature. Argon (purity: 99.9%) was used as the protective gas. The diamond micropowder was brazed at 1020 °C for 20 s and then naturally cooled. Thus, the brazed diamond micropowder bur fabricated is shown as Fig. 2.

## 2.3 Characterization of Physicochemical Properties

The portion with brazed diamond grits was cut and placed in aqua regia. The solution obtained was diluted using acetone after 24 h. The brazed diamond grits were gained by filter paper. The surfaces of both the bur and brazed diamond grits were observed using a JSM-6300 scanning electron microscope (SEM) coupled with energy dispersive x-ray spectroscopy (EDX) (JEOL Electronics Co., Ltd., Japan).

The bur was longitudinally cut. Its vertical section was first roughly ground, then finely ground and polished. Then, the section was wiped using an etching agent (absolute ethanol:nitric acid ( $1.4 \times 10^3$  kg/m<sup>3</sup>):hydrochloric acid ( $1.19 \times 10^3$  kg/m<sup>3</sup>) = 50 mL:50 mL:75 mL) for 3–5 s at room temperature. Finally, the section was cleaned with alcohol and observed using a XJL-03 upright metallurgical microscope (Nanjing Jiangnan Yongxin Optical Co., Ltd., PRC).

The phase analyses of the samples were carried out using a D/MAX-RB x-ray diffractometer (XRD) (Rigaku Corporation,



**Fig. 2** Brazed diamond micropowder bur

Japan). The incident ray was  $K_{\alpha}$  spectrum ( $\lambda_{K_{\alpha}} = 1.5406$  Å) of copper target. The scanning speed was 2°/min.

The melting point of the brazing alloy was measured using a DSC6300 thermal analyzer (NSK Ltd., Japan). The maximum testing range was set as 1200 °C.

## 2.4 Grinding Performance of Brazed Diamond Micropowder Bur

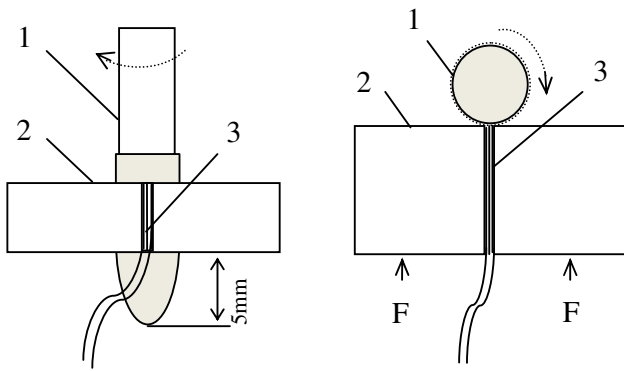
The grinding was carried out using a vertical driller (rotating speed: 560 rpm; main motor power: 4 kW). The ground material was a 6-mm-thick ceramic tile (shore hardness: 90). The brazed diamond micropowder bur with the same specification fabricated in a vacuum furnace was used as the control sample.

Figure 3 shows the schematic of the cylindrically ground ceramic tile using the brazed diamond micropowder bur. A thermocouple was clamped by two pieces of the ceramic tile, which were then fixed on the worktable with a groove. The thermocouple was made of a NiCr alloy foil (thickness: 0.1 mm; width: 1.5 mm) and a NiAl alloy foil (thickness: 0.1 mm; width: 1.5 mm), and a piece of insulating paper of 0.05 mm thick was placed in between them. The feeding force  $F$  was 30 N. In the first 15 min, the grinding temperature was recorded every 3 min. The chip was weighed every 10 min using a FA2004 electronic balance with an accuracy of 0.1 mg (Shanghai Liheng Instrument Co., Ltd., PRC). The roughness of the ground surface was measured using a A1535133 roughness tester with a sampling length of 0.8 mm (Shanghai Aice electron Co., Ltd., PRC).

## 3. Results and Discussion

### 3.1 Physicochemical Properties of Brazed Diamond Micropowder Bur

The Cr in the Ni-based brazing alloy is the main element that reacts with carbon on the diamond grit surface. Figure 4 shows the XRD spectrum of the Ni-based brazing alloy. The alloy was mainly composed of Ni-based solid solutions (Ni<sub>3</sub>Si, Ni<sub>3</sub>B) and CrB. Ni, Ni<sub>3</sub>Si, Ni<sub>3</sub>B and CrB conform to PDF # 04-0850, PDF # 32-0700, PDF # 19-0834 and PDF # 32-0277 in the International Centre for Diffraction Data (ICDD) files



**Fig. 3** Schematic of the cylindrically ground ceramic tile: (1) bur; (2) ceramic tile; (3) thermocouple

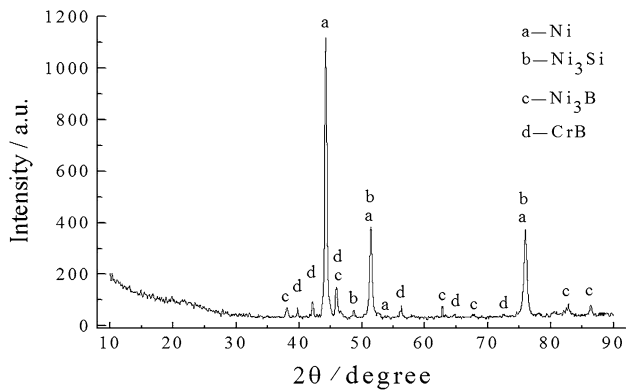


**Fig. 4** XRD spectrum of Ni-based brazing alloy

respectively. The melting of the brazing alloy includes both the melting of the Ni-based solid solution and the decomposition of the compounds.

Figure 5(a) shows the low-magnification image of the induction-brazed diamond micropowder bur. Unlike the even surface of the brazed diamond micropowder bur fabricated in a vacuum furnace (Ref 9), the surface of the induction-brazed diamond micropowder bur was fluctuant. The induction-brazed diamond micropowder grits distributed uniformly on the surface. The representative shape of a single of induction-brazed diamond micropowder grit is shown in Fig. 5(b). The induction-brazed diamond grit was well wetted by the brazing alloy and showed a certain outcropping.

When the brazing alloy was melted, the melting of the solid solution and the decomposition of the compounds produced an endothermic effect. Figure 6 shows the thermal analysis curve of the brazing alloy measured by differential scanning calorimetry (DSC).

B and Si are added in Ni-based brazing alloy to lower the melting temperature of the alloy and to broaden its melting range. There is a big solubility of Si in Ni matrix. The eutectic structure Ni-Ni<sub>3</sub>Si with the low melting point can be formed in the alloy. There is a small solubility of B in Ni matrix. The eutectic structure Ni-Ni<sub>3</sub>B with the low melting point can be formed in the alloy. Cr and B can form intermetallic compound CrB, which will decompose in the higher temperature. Three endothermic peaks at 977.2, 987.1, and 1012.2 °C appear in the thermal analysis curve (Fig. 6). They corresponded to the

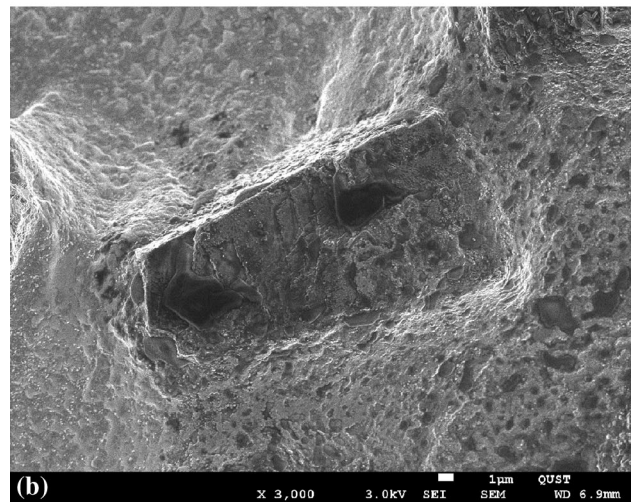
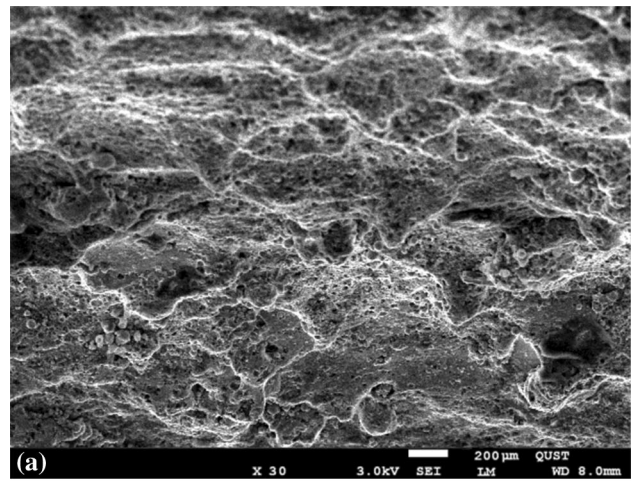


**Fig. 5** SEM images of induction-brazed diamond micropowder bur: (a) low-magnification image of induction-brazed diamond micropowder bur; (b) a single induction-brazed diamond micropowder grit

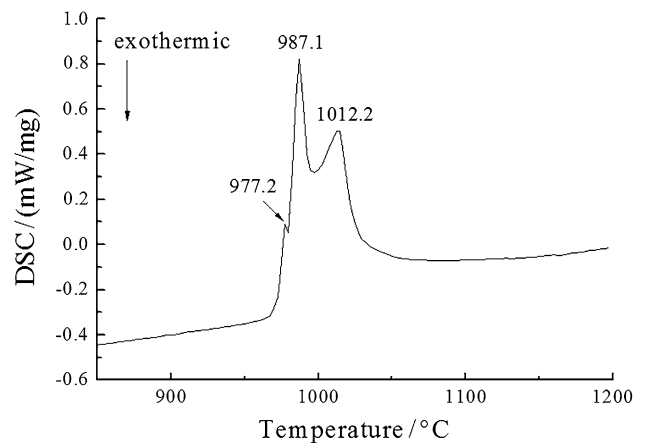


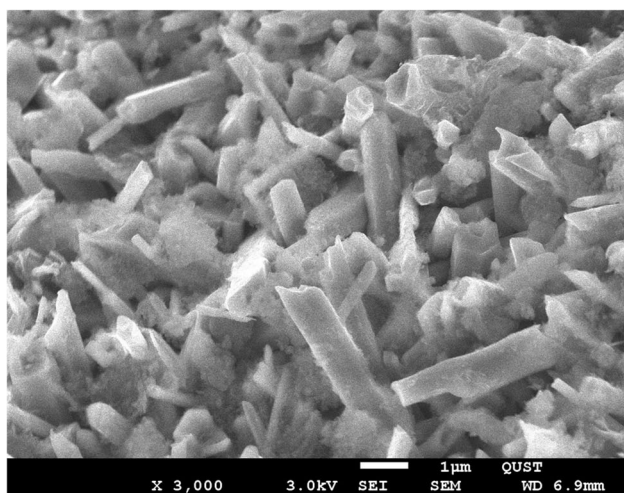
**Fig. 6** Thermal analysis curve of the brazing alloy measured by DSC

decomposition of Ni<sub>3</sub>Si, Ni<sub>3</sub>B, and CrB, respectively (Ref 10-12). The starting temperature of the first endothermic peak is approximately 970 °C. The finishing temperature of the third endothermic peak is approximately 1030 °C. No peak appeared

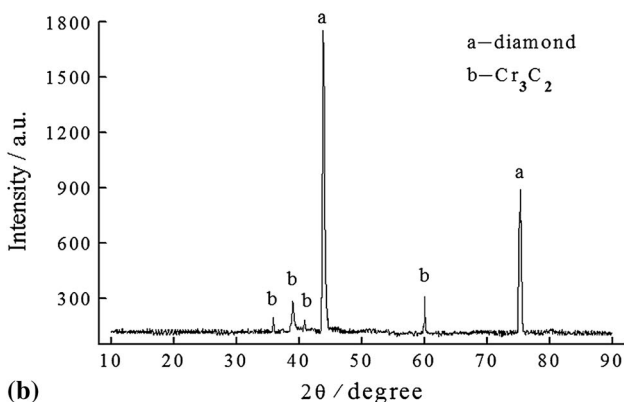
after the third peak. Therefore, the melting range of the Ni-based brazing alloy was between 970 and 1030 °C.

A brazing temperature of 1020 °C was adopted in this experiment. A part of the solid solution or compounds did not yet melt. The melt has a high viscosity and poor mobility (Ref 13, 14). At elevated temperature, the bur showed a high cooling speed owing to the small volume of the bur after the alternating magnetic field was stopped. The cooling speed reached up to 35 °C/s. Thus, the fluctuant surface of the liquid brazing alloy could be easily maintained. The morphology of the fluctuant surface varied because of the effect of the complicated alternating magnetic field.

Diamond and Cr-C compounds have a better chemical stability and difficult to solubilize in a strong acid. The brazed diamond micropowder bur was eroded when placed in aqua regia for 6 h, and the brazed diamond grits were gained by filter paper to observe the resulting surface using SEM. Figure 7(a) shows the morphology of the resulting brazed diamond grits. Irregular rod-like compounds are formed on the brazed diamond grits. The XRD spectrum shows that they are  $\text{Cr}_3\text{C}_2$  (Fig. 7b). Diamond and  $\text{Cr}_3\text{C}_2$  conform to PDF # 06-0675 and PDF # 35-0804 in ICDD files respectively. The formation of  $\text{Cr}_3\text{C}_2$  between the brazing alloy and diamond indicates the metallurgical bonding between them; therefore, the hold of the brazing alloy to the diamond grits was greatly enhanced (Ref 15).



(a)



(b)

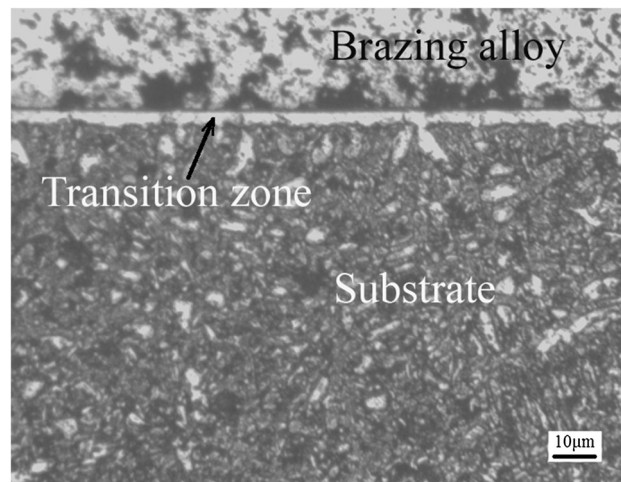
**Fig. 7** Typical interfacial morphology of the brazed diamond grits and their XRD spectrum: (a) morphology; (b) XRD spectrum

Figure 8(a) shows the microstructure near the interface of the brazing alloy and substrate. A three-layer structure was observed between them: brazing alloy, transition zone (TZ), and substrate. The energy dispersive spectrum of the TZ shows that it is formed by the elements in the brazing alloy (Ni, Cr, and Si) and those of substrate (Fe and C) (Fig. 8b). The formation of the TZ accounts for the outstanding metallurgical bonding between the brazing alloy and substrate (Ref 16).

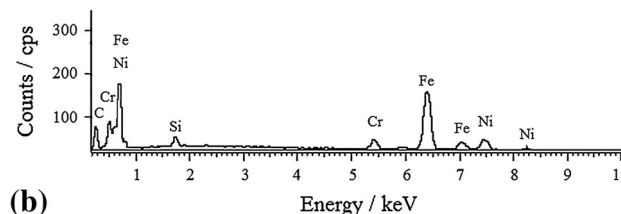
In summary, the diamond grits showed a fluctuant brazing alloy layer in the brazed diamond micropowder bur fabricated by supersonic frequency induction heating; metallurgical bonding was formed not only between the brazing alloy and diamond grits, but also between the brazing alloy and substrate. The fluctuant brazing alloy layer of the bur could store certain chips, thus increasing the grinding efficiency and improving the heat dissipation of the grinding arc area. Therefore, the life of the bur could be prolonged. Both the diamond grits and brazing alloy are difficult to fall off from the bur because they are now metallurgically bonded to the substrate.

### 3.2 Grinding Performance of the Brazed Diamond Micropowder Bur

The surface of the ceramic tile ground by the brazed diamond micropowder bur showed a low surface roughness because the size of the brazed diamond grits was small (30-40 μm), and only a part of the height of each brazed diamond grit protruded from the brazing alloy layer. All the measured values are between 0.09-0.12 μm for the roughness  $R_a$  of the surface of the ceramic tile cylindrically ground not only by the brazed diamond micropowder bur fabricated by induction heating, but also by that fabricated in a vacuum furnace.



(a)



(b)

**Fig. 8** Microstructure of the interface of brazing alloy and substrate (a) and energy dispersive spectrum of transition zone (b)

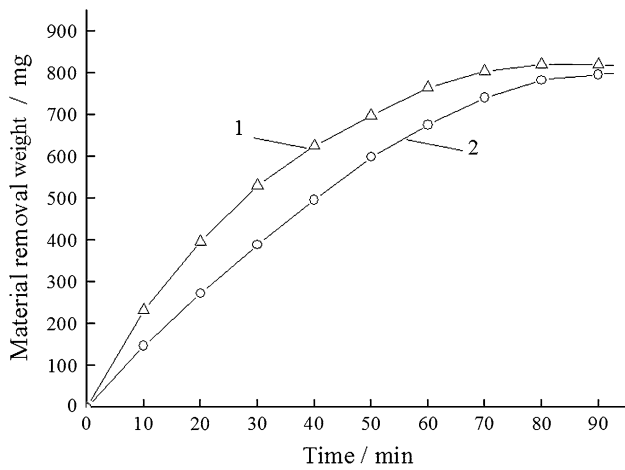


**Fig. 9** Weight of removed material from the cylindrically ground ceramic tile: (1) by the brazed diamond micropowder bur fabricated by induction heating; (2) by the brazed diamond micropowder bur fabricated in a vacuum furnace

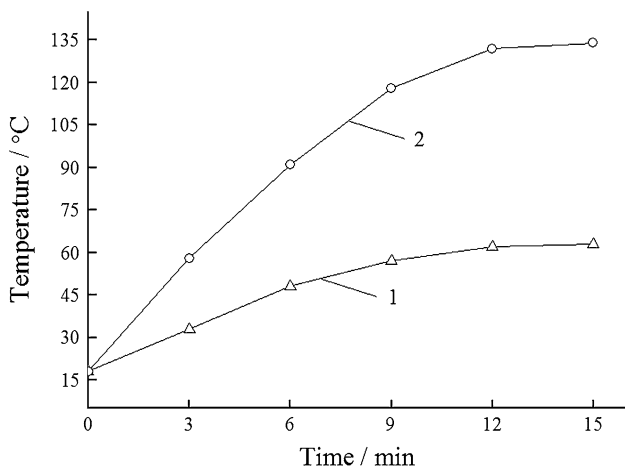


**Fig. 10** Temperature of the grinding arc area of the cylindrically ground ceramic tile: (1) by the brazed diamond micropowder bur fabricated by induction heating; (2) by the brazed diamond micropowder bur fabricated in a vacuum furnace

Figure 9 shows the weight of the removed material from the cylindrically ground ceramic tile. Owing to its large chip space, the weight of the removed material from the ceramic tile ground by the brazed diamond micropowder bur fabricated by induction heating is higher than that ground by the brazed diamond micropowder bur fabricated in a vacuum furnace in the first 90 min. Afterwards, the weight of the removed material became equal because of the damage to the abrasive particles.

Figure 10 shows that the temperature of the grinding arc area of the cylindrically ground ceramic tile by the brazed diamond micropowder bur at room temperature (20 °C). The temperature of the grinding arc area is under 70 °C when the ceramic tile was cylindrically ground using the brazed diamond micropowder bur fabricated by induction heating. This is because the fluctuant surface of the bur could well dissipate the heat. The temperature of the grinding arc area increased to 100 °C after 7 min when the ceramic tile was cylindrically ground using the brazed diamond micropowder bur fabricated

in a vacuum furnace, thus preventing its use in some cases such as long-time dental work.

#### 4. Conclusion

A fluctuant surface was formed on the brazing alloy layer of the brazed diamond micropowder bur fabricated by supersonic frequency induction heating. The brazed diamond grits with a certain outcropping distributed uniformly on the brazing alloy layer. The brazing alloy was metallurgically bonded to both the diamond grits and substrate.

A surface roughness of 0.09-0.12  $\mu\text{m}$  ( $R_a$  value) was generated on the surface of the cylindrically ground ceramic tile by the brazed diamond micropowder bur fabricated by induction heating.

A large chip space was observed in the brazed diamond micropowder bur fabricated by supersonic frequency induction heating. In the first 90 min, the weight of the removed material from the ceramic tile ground by the brazed diamond micropowder bur fabricated by induction heating was higher than that ground by the brazed diamond micropowder bur fabricated in a vacuum furnace. Afterwards, the weights of the removed material became close because of the damage to the abrasive particles.

An outstanding heat dissipation was observed for the brazed diamond micropowder bur fabricated by supersonic frequency induction heating. The grinding arc area temperature was below 70 °C during the cylindrical grinding of the ceramic tile by the brazed diamond micropowder bur fabricated by induction heating.

#### Acknowledgments

We would like to acknowledge the financial support of Natural Science Foundation of Shandong Province of P. R. China (Grant No. ZR2010EM015).

#### Reference

1. S. Buhl, C. Leinenbach, R. Spolenak, and K. Wegener, Influence of the Brazing Parameters on Microstructure, Residual Stresses and Shear Strength of Diamond-Metal Joints, *J. Mater. Sci.*, 2010, **45**(16), p 4358–4368
2. W.Q. Qiu, Z.W. Liu, L.X. He, D.C. Zeng, and Y.W. Mai, Improved Interfacial Adhesion between Diamond Film and Copper Substrate Using a Cu (Cr)-diamond Composite Interlayer, *Mater. Lett.*, 2012, **81**(15), p 155–157
3. S.F. Huang, H.L. Tsai, and S.T. Lin, Effects of Brazing Route and Brazing Alloy on the Interfacial Structure Between Diamond and Bonding Matrix, *Mater. Chem. Phys.*, 2004, **84**(2-3), p 251–258
4. B.J. Ma and Q.X. Yu, Hot-Filament Chemical Vapor Deposition of Amorphous Carbon Film on Diamond Grits and Induction Brazing of the Diamond Grits, *Appl. Surf. Sci.*, 2012, **258**(10), p 4750–4755
5. W.F. Ding, J.H. Xu, Z.Z. Chen, C.Y. Yang, C.J. Song, and Y.C. Fu, Fabrication and Performance of Porous Metal-bonded CBN Grinding Wheels Using Alumina Bubble Particles as Pore-forming Agents, *Int. J. Adv. Manuf. Technol.*, 2013, **67**(5-8), p 1309–1315
6. H. Onishi, M. Kobayashi, A. Takata, K. Ishizaki, T. Shioura, Y. Kondo, and A. Tukuda, Fabrication of New Porous Metal-bonded Grinding Wheels by HIP Method and Machining Electronic Ceramics, *J. Porous Mater.*, 1997, **4**(3), p 187–198
7. Y. Fautrelle, D. Perrier, and J. Etay, Free Surface Controlled by Magnetic Fields, *ISIJ Int.*, 2003, **43**(6), p 801–806

8. A.Y. Deng, E.G. Wang, Y.Y. Xu, X.W. Zhang, and J.C. He, Experimental Research on Melting Surface behavior in Mold under Compound Magnetic Field, *Acta Metall. Sinica*, 2010, **46**(8), p 1018–1024
9. C.M. Sung, Brazed Diamond Grid: A Revolutionary Design for Diamond Saws, *Diamond Relat. Mater.*, 1999, **8**(8-9), p 1540–1543
10. J. Ruiz-Vargas, N. Siredey-Schwaller, N. Gey, P. Bocher, and A. Hazotte, Microstructure Development During Isothermal Brazing of Ni/BNi-2 Couples, *J. Mater. Process. Technol.*, 2013, **213**(1), p 20–29
11. K.P. Gupta, The Cr-Ni-Si (Chromium-Nickel-Silicon) System, *J. Phase Equilib. Diffus.*, 2006, **27**(5), p 523–528
12. T. Tokunaga, K. Nishio, and M. Hasebe, Thermodynamic Study of Phase Equilibria in the Ni-Si-B System, *J. Phase Equilib.*, 2001, **22**(3), p 291–299
13. G.B. Mi, P.J. Li, P.S. Popel, N.Y. Konstantinova, and L.J. He, Structure and Property of Metal Melt III—Relationship between Kinematic Viscosity and Size of Atomic Clusters, *Sci. China Phys. Mech. Astron.*, 2010, **53**(11), p 2054–2058
14. S.N. Maiti and P.K. Mahapatro, Melt Rheological Properties of Nickel Powder Filled Polypropylene Composites, *Polym. Compos.*, 1988, **9**(4), p 291–296
15. C. Artini, M.L. Muolo, and A. Passerone, Diamond-metal Interfaces in Cutting Tools: A Review, *J. Mater. Sci.*, 2012, **47**(7), p 3252–3264
16. B.J. Ma and F. Lian, Study on the Use of CuSnTi Brazing Alloy for Induction Brazing of Diamond Grits Surface-treated by Direct Current Plasma Chemical Vapor Deposition, *Int. J. Refract. Met. Hard Mater.*, 2013, **41**, p 339–344